Altitude Distribution of the Auroral Acceleration Potential Determined from Cluster Satellite Data at Different Heights

Göran T. Marklund,[1] Soheil Sadeghi,[1] Tomas Karlsson,[1] Per-Arne Lindqvist,[1] Hans Nilsson,[2] Colin Forsyth,[3] Andrew Fazakerley,[3] Elizabeth A. Lucek,[4] and Jolene Pickett[5]

[1]*Space and Plasma Physics, School of Electrical Engineering, KTH, SE 10044 Stockholm, Sweden*
[2]*Swedish Institute of Space Physics, Box 812, SE 981 28 Kiruna, Sweden*
[3]*Mullard Space Science Laboratory, University College, Holmbury St Mary, Dorking, Surrey RH5 6NT, United Kingdom*
[4]*Space and Atmospheric Physics Group, Blacket Laboratory, Imperial College, London, United Kingdom*
[5]*Department of Physics and Astronomy, University of Iowa, Iowa City, Iowa 52242-1479 USA*

(Received 11 October 2010; published 1 February 2011)

Aurora, commonly seen in the polar sky, is a ubiquitous phenomenon occurring on Earth and other solar system planets. The colorful emissions are caused by electron beams hitting the upper atmosphere, after being accelerated by quasistatic electric fields at 1–2 R_E altitudes, or by wave electric fields. Although aurora was studied by many past satellite missions, Cluster is the first to explore the auroral acceleration region with multiprobes. Here, Cluster data are used to determine the acceleration potential above the aurora and to address its stability in space and time. The derived potential comprises two upper, broad *U*-shaped potentials and a narrower *S*-shaped potential below, and is stable on a 5 min time scale. The scale size of the electric field relative to that of the current is shown to depend strongly on altitude within the acceleration region. To reveal these features was possible only by combining data from the two satellites.

DOI: 10.1103/PhysRevLett.106.055002 PACS numbers: 94.20.wh, 06.30.Gv, 92.60.hw, 94.30.Kq

Introduction.—Between Earth's magnetosphere and the upper atmosphere at high latitudes, there is a continuous flow and exchange of energy and momentum, carried by energetic particles, currents, and waves, towards and away from Earth, guided by Earth's magnetic field. As part of this process, intense quasistatic electric fields and associated potential drops aligned with Earth's magnetic field are formed, governed by the requirements of charge neutrality and current continuity in the space plasma. The term quasistatic is used to describe that the structures are stable on a time scale long compared to the time needed for a charged particle to pass the structure. The region where such parallel electric fields are formed is known as the auroral acceleration region (AAR), typically located between 4000 and 12 000 km above the polar atmosphere [1]. Aurora and the associated acceleration processes are ubiquitous space plasma processes, occurring throughout the solar system, such as around Jupiter and Saturn. The suggestion that electric fields, aligned with Earth's magnetic field lines, accelerate particles producing aurora was first made by Hannes Alfvén [2]. Since then it has been well confirmed experimentally by satellite and rocket measurements. The parallel electric fields occur together with converging or diverging electric fields perpendicular to the magnetic field, in *U*-shaped potential structures [3,4], or together with monopolar (one-directional) electric fields in *S*-shaped potential structures [5,6]. Figure 1 illustrates *U*-shaped potential structures above the aurora, extended along the direction of Earth's magnetic field. The electric fields in the upper parts of the structures are oriented perpendicular to the magnetic field. In the lower parts the electric fields are instead directed parallel or antiparallel to the magnetic field. Negative potential structures are associated with upward currents and upward electric fields, accelerating electrons downwards, producing intense aurora and ion beams moving away from Earth. Positive potential structures (center) may develop in the downward current region. They are associated with a downward parallel electric field [6–8], accelerating electrons away from, and ions towards Earth, up to energies of a few

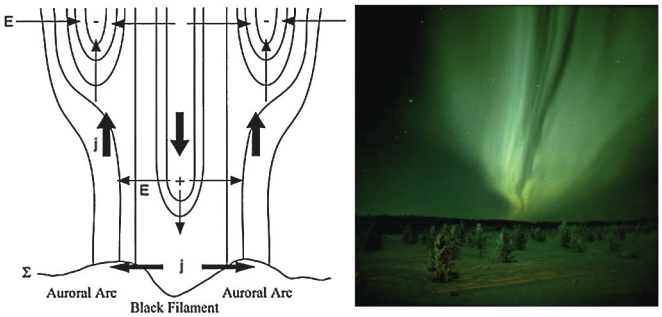

FIG. 1 (color). A schematic of the electric field and current system (left) representative of two parallel arcs (right) in upward current regions, separated by dark bands in regions of downward current. The arcs are produced by high-energy electrons colliding with the upper atmosphere, after being accelerated by an upward directed parallel electric field at altitudes around one Earth radius. Above the dark areas, a downward directed electric field accelerates electrons away from Earth, corresponding to a downward current. How the parallel electric fields and potential drops are distributed in altitude is studied here, for the first time using Cluster multiprobe data obtained at different heights of the AAR.

keV. This acceleration occurs at lower altitudes, between 1000 and 4000 km [6].

Different mechanisms for maintaining parallel electric fields have been proposed, such as strong double layers [9], weak double layers [10], Alfvén waves [11], magnetic mirror supported fields [12,13] and anomalous resistivity [14]. Experimental evidence of parallel electric fields has been presented from sounding rockets [15] and satellites such as Polar [16] and FAST [17–19]. How the parallel electric fields and potential drops are distributed in altitude and how stable they are in space and time cannot be determined from single-satellite observations. Numerical simulation results for the upward current region indicate that the parallel electric fields are concentrated in two layers between 1 and 2 R_E, a more stable electron transition layer and, above this, a more dynamic ion layer accounting for most of the total acceleration potential [18]. Although the aurora was studied by several single-satellite missions in the past, such as Viking, Freja, Akebono, Polar, FAST [1], the instantaneous morphology of the AAR, such as the altitude distribution of the acceleration potential and its stability, requires simultaneous multipoint data to be resolved. This became an opportunity when the Cluster orbits were lowered in late 2008, enabling frequent crossings of the AAR. The observations presented here were obtained by the Cluster 1 and 3 spacecraft, crossing the AAR of large-scale aurora associated with upward currents near dusk. Figure 2 illustrates the trajectories of the two spacecraft, separated in altitude by 2600 km at this time. The Cluster data presented here were obtained by the EFW electric field and wave [20], FGM magnetic field [21], PEACE electron [22], and CIS ion [23] instruments.

Cluster 3 and Cluster 1 observations, at altitudes of 1 and 1.4 R_E, respectively.—Figure 3 (left) presents Cluster 3 data obtained between 16:55 and 17:15 UT on a duskside oblique oval crossing at an altitude of 1 R_E or 6400 km. The acceleration signatures of interest are seen between 17:00 and 17:03 UT, indicated by the blue vertical lines. Enhanced fluxes of down-going electrons with inverted-V energy distributions (so called since the shape resembles an inverted V) are seen in two regions, of about 100 and 150 km widths (mapped along the geomagnetic field to 100 km altitude) and peak energies of 4 and 5 keV, respectively, (panel 1). The wider electron distribution coincides with: a beam of upward moving ions with peak energies of 2.5 keV (panel 2), a localized, intense electric field, directed southward and peaking at 200 mV/m (panel 3), associated with a steplike increase of the electric potential of 3 kV (panel 5) and a weak plasma density cavity (panel 6). The accelerated down-going electrons are seen where the tangential magnetic field has a negative slope, indicative of an upward current. The two inverted-V electron distributions are signatures of two adjacent U-shaped potential structures, with acceleration potentials of 4 and 5 kV located above Cluster 3, accelerating electrons downwards, over regions of 100 and 150 km widths (mapped to 100 km altitude), respectively.

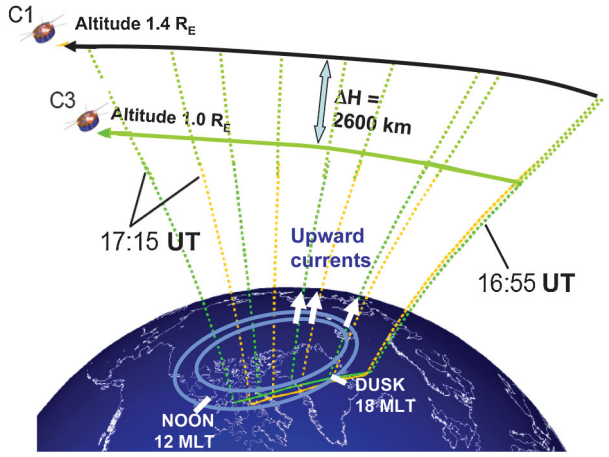

FIG. 2 (color). Schematic view of the Cluster C3 and C1 satellite trajectories between 16:55 and 17:15 UT on 5 June 2009, crossing the AAR of dusk-side aurora at altitudes of 1 and 1.4 R_E, respectively. The blue ovals indicate the poleward half of the auroral oval, which is characterized by upward and downward currents for the dusk-side and dawn-side magnetic local time sectors, respectively.

The acceleration potential below Cluster 3 has been inferred in two ways: from the peak energy of the up-going ions of 2.5 keV (panel 2) and from the steplike potential increase of 3 kV (panel 5), being consistent within the uncertainties of about 20%, inherent in the estimations of these parameters.

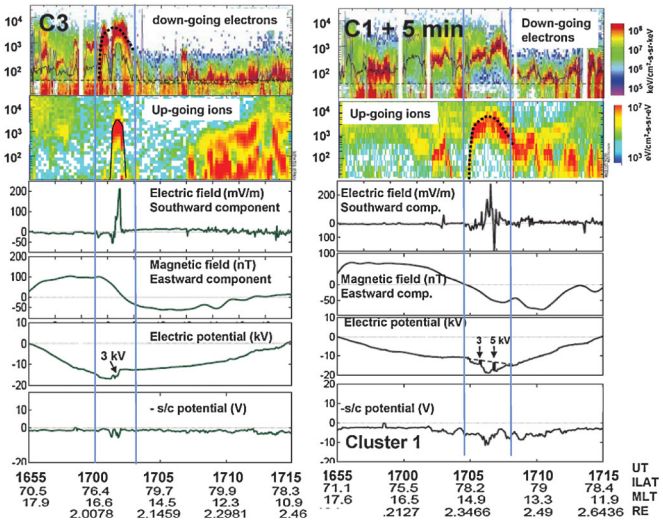

FIG. 3 (color). Cluster 3 data at 1 R_E (left) and Cluster 1 data at 1.4 R_E (right) between 16:55 and 17:15 UT. The panels show, from the top: (1) energy spectrograms of down-going electrons; (2) energy spectrograms of up-going ions, the peak energy given by the solid black curve; (3) the electric field component perpendicular to the geomagnetic field **B** and normal to the oval,~ the southward component; (4) the residual magnetic field component tangential to the oval,~ the eastward component; (5) the potential, integrated from the electric field along the trajectory; (6) the negative of the spacecraft potential, indicating relative plasma density variations.

Figure 3 (right) presents Cluster 1 data at 1.4 R_E (9000 km) for the same time period and using the same format. The acceleration signatures of interest are seen between 17:04:45 and 17:08 UT, indicated by the blue vertical lines. The down-going electron distributions are also here indicative of two regions, of 120 and 140 km widths (mapped to 100 km altitude) with peak energies of 0.4 keV and 1 keV, respectively, (panel 1). These coincide with enhanced fluxes of up-going ions, with representative peak energies of 4 and 5 keV for the two regions (panel 2), and with a broad and irregular electric field structure (panel 3).

The electric field reverses direction several times, peaking at +250 mV/m (southward field) and −150 mV/m (northward field) and is associated with a large-scale negative potential drop, with typical values of 3 and 5 kV for the two regions, respectively, (panel 5). These features occur within a broad region of upward current and with a broad and irregular plasma density cavity (panel 6), characteristic of the acceleration region. The two inverted-V electron distributions suggest that Cluster 1 crossed two U-shaped potential structures, with acceleration potentials of 0.4 and 1 kV, respectively, located above Cluster 1, accelerating electrons downwards, over regions of 120 and 140 km, respectively. The acceleration potential below Cluster 1, has been inferred from the peak energies of the up-going ions at the centers of the two U-shaped structures, being 4 and 5 keV, respectively, (panel 2) as well as from the corresponding electric potential drops from the ambient level (indicated by the dotted line) of 3 and 5 kV, respectively, the estimates agreeing within the 20% relative uncertainties.

Synthesis, discussion, and conclusions.—A synthesis of the Cluster 1 and 3 observations is presented in Fig. 4, showing the altitude distribution of the acceleration potential above the high-latitude aurora, being consistent with the Cluster 3 data in the lower part of AAR at 1.0 R_E, and with the Cluster 1 data in the upper part of the AAR at 1.4 R_E. The upper and central parts of the derived acceleration potential pattern is composed of two roughly equal U-shaped potential structures (indicated by 1 and 2 in red), with acceleration potentials of about 4 kV, distributed between 1.0 and 1.4 R_E. The lower part of the pattern is characterized by an S-shaped potential (indicated by 3 in red) with an acceleration potential of 3 kV, located below 1 R_E, and centered directly below structure 2. For a quasi-static U-shaped potential structure, the potential drop, $\Delta\Phi_\perp$, derived by integrating the perpendicular electric field along the spacecraft trajectory, should equal $\Delta\Phi_{ll}{}^i$, the acceleration potential inferred from the characteristic energy of the up-going ions, as is also found to be the case here. For S-shaped potential structures, the relation between $\Delta\Phi_\perp$ and $\Delta\Phi_{ll}{}^i$ is more complicated and depends on its morphology and is therefore not necessarily described by equality. The $\Delta\Phi_\perp$ and $\Delta\Phi_{ll}{}^i$ values for the S-shaped structure traversed by Cluster 1 were 3 and 2.5 kV, respectively, consistent with the fact that $\Delta\Phi_\perp$ should be an upper limit for $\Delta\Phi_{ll}{}^i$.

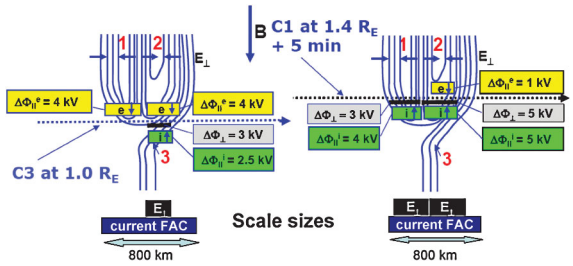

FIG. 4 (color). Altitude distribution of the acceleration potential, presented in terms of equipotential contours (spacing 1 kV), derived by combining Cluster 3 and 1 data. The pattern consists of two upper and broad U-shaped potential structures (1 and 2) and a narrower S-shaped potential structure (3) located below. The small boxes indicate the widths of the down-going electron (yellow) and up-going ion (green) distributions. The black bold lines in between, indicate where the electric potential deviated much from the ambient level. The larger attached boxes present acceleration potential estimates. For the region above the spacecraft, the acceleration potential, $\Delta\Phi_{ll}{}^e$, is inferred from the down-going electron energy (yellow). For the region below the spacecraft, the acceleration potential is estimated from the potential drops, $\Delta\Phi_\perp$ (grey), and from $\Delta\Phi_{ll}{}^i$, given by the peak ion energy (green). The vertical potential drops remained stable at 4 kV at the position of structure 1, and between 6 and 7 kV at the position of structure 2. The total structure (or current) width also remained stable, 800 km for both spacecraft, scaled to their mean altitude. Note also that the scale size of the electric field relative to that of the current was much smaller on Cluster 3, but roughly equal for Cluster 1.

A requirement for tying together the observations at different altitudes by the two Cluster spacecraft, as has been done here, is that the acceleration potential distribution was stable on the time scale corresponding to the separation between the two spacecraft, i.e., about 5 min. One way to illustrate the stability is by the maximum vertical potential drops at the center of the two U-shaped structures, which remains stable at 4 kV for structure 1, and between 6 and 7 kV for structure 2. Also, the observed widths and peak energies of the up-going ions observed by Cluster 1 match those of the down-going electrons observed by Cluster 3 in the lower part of the acceleration region, as illustrated by the dotted curve fitted to the Cluster 1 ion data (Fig. 3, right, panel 2) being superposed on the Cluster 3 electron data (Fig. 3, left, panel 1) where account has been taken of how the width scales between the altitudes of the two spacecraft.

The importance of using multisatellite, as compared to single-satellite, observations for studying the spatiotemporal nature of the AAR, can be illustrated by considering what the interpretation had been if data were available only from one single spacecraft. Based on Cluster 1 data only, the combined electron, ion, and electric field signatures would be interpreted in terms of two typical U-shaped potential structures formed within the upward current

region above the aurora. Based on Cluster 3 data only, the one-directional electric field spike and correlated up-going ion beam would be interpreted in terms of the other common type of acceleration structure, an asymmetric *S*-shaped potential. The pattern derived here shows that both of these types of acceleration potential structures appear together as parts of a combined structure, with the two *U*-shaped potentials (1 and 2) dominating its upper and central parts, between 1 and 1.4 R_E, and the acceleration potential of the *S*-shaped structure (3) located in its lower parts and connected to the flank of the combined structure. *S* potentials occur typically at sharper plasma boundaries than for *U* potentials [24,25]. Thus, it seems reasonable that for a combined potential structure of the kind derived here, the *S* potential should be connected to the flanks of the structure, where the plasma gradients are most pronounced.

The distinctly different acceleration signatures seen by Cluster 1 and Cluster 3, in the upper and lower part of the acceleration region, can be illustrated by the electric field, potential, and satellite potential data. Cluster 1 observes a very broad and irregular electric field structure, associated with a large-scale potential well and a broad and deep plasma density cavity, the scales of which are comparable to the width of the upward magnetic field-aligned current or of the potential structure as a whole. For Cluster 3, the intense electric field and the associated steplike increase in the potential and the plasma density cavities are more localized features (as indicated by the thick black line below the Cluster 3 orbit), significantly smaller than the width of the upward magnetic field-aligned current or the structure as a whole. That the electric field structure is significantly smaller than the current sheet, as shown by the Cluster 3 data, is a common but not clarified feature, observed by numerous satellites in the past. The pattern derived here shows how the scale size of the electric field relates to that of the current, being much smaller in the lower parts, and roughly equal, in the upper parts of the AAR, respectively, revealing the strong altitude dependence of the acceleration potential within the AAR.

This unique opportunity with the Cluster spacecraft 1 and 3 probing the acceleration region in its upper and lower parts separated in time by only five minutes enabled the altitude distribution of the acceleration potential within the AAR to be resolved, which has not been done before. The good match between observed widths and characteristic energies of the down-going electrons (observed by Cluster 3), and those of the up-going ions (observed by Cluster 1), implies that the acceleration potentials of two dominating *U*-shaped structures were confined in altitude between the two spacecraft, and moreover that the structure was stable on a 5 min time scale. This is also supported by the fact that the maximum vertical potential drops at the center of the two *U*-shaped structures, as well as the width of the combined structure, remained stable between the two crossings. Strong candidates for the maintenance of the quasistatic parallel electric fields and potential structures derived here are strong double layers [9] and/or magnetic mirror supported fields [12,13], although the data available do not allow us to clearly distinguish between these, or to exclude any of the other mechanisms discussed above.

The author is grateful to a large number of people who have contributed to the Cluster mission. The Cluster project was supported by the European Space Agency and NASA. Project support has also been provided by a grant from NASA Goddard Space Flight Center to the University of Iowa. This study has been supported by the Swedish National Space Board and by Space and Plasma Physics, School of Electrical Engineering, KTH, Stockholm.

[1] G. Paschmann, S. Haaland, and R. Treumann, *Auroral Plasma Physics*, Space Sciences Series of ISSI (Kluwer Academic Publishers, Dordrecht, 2003).
[2] H. Alfvén, Tellus **10**, 104 (1958).
[3] P. Carlqvist and R. Boström, J. Geophys. Res. **75**, 7140 (1970).
[4] F. S. Mozer *et al.*, Space Sci. Rev. **27**, 155 (1980).
[5] P. Mizera, D. Gorney, and J. Fennell, J. Geophys. Res. **87**, 1535 (1982).
[6] G. Marklund, T. Karlsson, and J. Clemmons, J. Geophys. Res. **102**, 17 509 (1997).
[7] G. T. Marklund *et al.*, Geophys. Res. Lett. **21**, 1859 (1994).
[8] G. Marklund *et al.*, Nature (London) **414**, 724 (2001).
[9] L. Block, Cosmic Electrodyn. **3**, 349 (1972).
[10] M. Temerin *et al.*, Phys. Rev. Lett. **48**, 1175 (1982).
[11] Y. Song and R. L. Lysak, Space Sci. Rev. **95**, 273 (2001).
[12] S. Knight, Planet. Space Sci. **21**, 741 (1973).
[13] Y. T. Chiu and M. Schultz, J. Geophys. Res. **83**, 629 (1978).
[14] M. Hudson, and F. S. F. Mozer, Geophys. Res. Lett. **5**, 131 (1978).
[15] F. S. Mozer and P. Bruston, J. Geophys. Res. **72**, 1109 (1967).
[16] F. S. Mozer and C. A. Kletzing, Geophys. Res. Lett. **25**, 1629 (1998).
[17] R. E. Ergun *et al.*, Geophys. Res. Lett. **27**, 4053 (2000).
[18] R. E. Ergun *et al.*, Phys. Plasmas **9**, 3685 (2002).
[19] L. Andersson *et al.*, Phys. Plasmas **9**, 3600 (2002).
[20] G. Gustavsson *et al.*, Space Sci. Rev. **79**, 137 (1997).
[21] A. Balogh *et al.*, Space Sci. Rev. **79**, 65 (1997).
[22] A. Johnstone *et al.*, Space Sci. Rev. **79**, 351 (1997).
[23] H. Réme *et al.*, Space Sci. Rev. **79**, 303 (1997).
[24] G. Marklund *et al.*, Nonlinear Proc. Geophys. **11**, 709 (2004).
[25] T. Johansson *et al.*, Ann. Geophys. **24**, 1713 (2006).